JOURNAL OF PROPULSION AND POWER
Vol. 11, No. 6, November–December 1995

Mixing Characteristics of Twin Impinging Circular Jets

P. J. Disimile*
University of Cincinnati, Cincinnati, Ohio 45221-0070
and
E. Savory† and N. Toy‡
University of Surrey, Guildford GU2 5XH, England, United Kingdom

The mixing region of two identical incompressible air jets was studied at included angles of 30 and 45 deg using total pressure surveys and quantitative flow visualization. This work has confirmed that, while the rates of decay of centerline total pressure are similar for both configurations, the growth of the 45-deg jets after impingement in the plane normal to the nozzle plane is over 52% greater than in the 30-deg case. However, in the nozzle plane the growth rates for both cases are almost identical to that of a single jet. This growth pattern produced an elliptical mixing cross section with the major axis over 2.5 times larger than the minor axis for the 45-deg case and approximately 1.6 times larger for the 30-deg jet configuration. Image analysis of the visualization studies has also shown that the half-widths of the jets grow at the same rate as the overall width of the interface region between the jet and the external fluid.

Nomenclature

b_1 = pressure profile half-width measured at $\frac{1}{2}P_{t\max}$ of the impinging jets in the plane of impingement, Y direction
b_2 = pressure profile half-width measured at $\frac{1}{2}P_{t\max}$ of the impinging jets normal to the plane of impingement, Z direction
D = nozzle diameter
P_t = total pressure
P_{te} = jet exit total pressure
$P_{t\max}$ = maximum total pressure at a given cross section
Re = Reynolds number, $U_e^* D/\nu$
U_e = jet exit velocity
X = longitudinal (jetwise) Cartesian coordinate
X_0 = geometrical distance to twin jet impingement
Y = lateral Cartesian coordinate
Z = vertical Cartesian coordinate
θ = impingement angle
η = Y/b_1 or Z/b_2
ν = kinematic viscosity

Introduction

THE interaction between combustion stability and injector configuration is an important consideration in the design of an injector nozzle. The geometrical characteristics of such an injector can significantly affect the flame stability for that design. In general, the basic nozzle configurations used for delivering fuel and oxidizers can be described as follows: 1) unlike-impinging jets, where the fuel and the oxidizer are delivered separately and the two fluids impinge together; 2) like-impinging jets, where either the fuel or the oxidizer is delivered by the nozzles and these jets then impinge together and combine with the other fluid; and 3) nonimpinging jets, where the fluid is delivered into the combustion chamber without impingement.

In the first case, the resulting complex flowfield may be considered to be unstable and easily excited to instability. However, in the second case, for like-impinging jets the flowfield is far more stable and not easily disturbed. Finally, for the third case, the flowfields do not impinge and are, therefore, highly stable. The like-impinging-type nozzles provide fluid interaction between similar propellants and this arrangement is usually of the twin nozzle configuration. Here, the two like fluid streams are angled inward such that they impinge on one another at a point, producing an elliptical fan-shaped spray of droplets. The distance from the nozzle exits to the geometrical point of impingement is known as the impingement length X_0. Because both streams are of the same propellant there is no mixing in this fan. However, energy dissipated by the interaction of the two liquid jets atomizes the liquid producing a fine distribution of fluid particles.

Like-impinging jets are frequently used for liquid/liquid propellant systems in which reaction or heat transfer between unlike-impinging streams is undesirable. Although the initial mixing provided by the injector configuration is poorer than for the unlike-impinging cases, the like-impinging configuration avoids most of the reactive stream demixing of unlike-impinging jet designs and maintains the combustion stability better than the complex flows associated with the unlike-impinging jets.

Previous work[1–5] concerning twin impinging jets is limited to only a few studies of air jets in which the mean velocity and turbulence quantities were measured for different impingement angles and for both equal and unequal jet exit velocities. The present authors carried out an earlier study[6] in which twin impinging jets in air and dye jets in water were examined using quantitative digital analysis of smoke and LIF laser induced fluorescence (LIF) visualization. The angles of impingement considered in that work were 30 and 45 deg. However, in order to better understand the mixing that takes place in like-impingement flows, the following, more detailed study was initiated using twin air jets issuing into still air. Since a major issue of interest to the gas–turbine community is the rate of spread of these jets and the resulting degree of mixing that ensues the research has concentrated upon those aspects of the flowfield.

Experimental Strategy

The present study is comprised of two parts. First, the structure of the mixing region interface between the impinging

Received June 25, 1994; revision received Feb. 4, 1995; accepted for publication Feb. 11, 1995.

*Bradley Jones Associate Professor, Aerospace Engineering, ML70. Member AIAA.
†Lecturer, Department of Civil Engineering.
‡Professor of Fluid Mechanics, Department of Civil Engineering.

jets and the surrounding air was examined using qualitative smoke visualization and image processing. Secondly, the mixing flows were studied using measurements of total pressure profiles both before and after the impingement point. The experimental arrangements for the two cases will now be described.

Smoke Visualization

The experimental arrangement for the quantitative analysis of smoke flow visualization is illustrated in Fig. 1. The smoke was produced by evaporation from a commercial generator, using food grade mineral oil, with an average particle diameter of 0.55 μm. In fact, 90% of all particles were below 1 μm and the remainder below 5 μm. Hence, the particles closely follow the mean airflow. Also, estimates using Stokes law with the Cunningham correction, indicated that these particles will respond to 90% of the amplitude of any velocity fluctuations up to a frequency of 22 kHz. The generator was connected to a small centrifugal fan and then, via a plenum chamber, to a twin-jet arrangement incorporating copper nozzles. The cross-sectional area of these nozzles was constant with D of 20 mm and a U_e of 5.6 m/s for each nozzle, giving a $Re = 7.5 \times 10^3$ based on D. The flow rate through each nozzle was balanced and controlled using separate needle valves located inside the plenum chamber.

The included angle θ between the two jet nozzles was set to 30 deg in the first set of experiments and then modified to 45 deg, and the measurements repeated. However, in each case the nozzle spacing was varied in order to produce the same X_0 of $10.33D$, which was that utilized by Rho et al.[2] The nozzle arrangement was mounted with the jets angled vertically downwards in order to minimize buoyancy effects in the flow visualization experiments. The distance from the nozzle exit to the ground was approximately $150D$, which was considered to be sufficiently far downstream so as to not affect the behavior of the jets within the region of interest between the jet exit and $30D$ downstream.

Light sheet visualization tests were conducted within a darkened laboratory. The light sheet was produced using a tungsten halogen lamp and a narrow slit. Initially, light sheet experiments were performed to determine the overall qualitative features of the flowfield. All flowfield images were recorded on video tape and selected images photographed. Figures 2 and 3 present the flowfield viewed in the XZ plane for the 30- and 45-deg nozzle orientation (see Fig. 1). Figure 4 provides a view of the XY development of the 30-deg nozzle configuration.

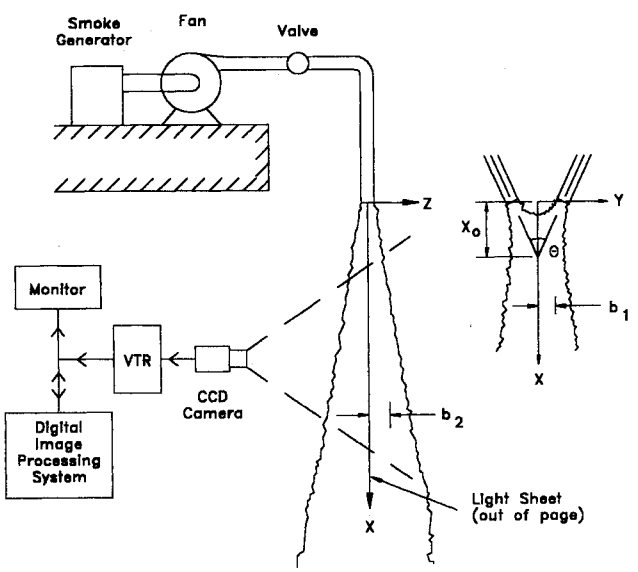

Fig. 1 Diagrammatic representation of the twin jets.

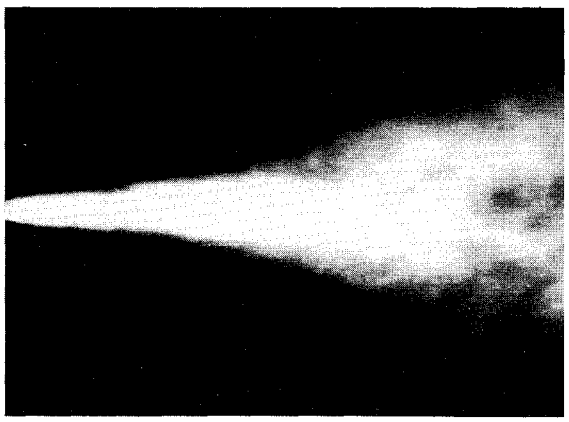

Fig. 2 Flow visualization as viewed from the XZ plane for the 30-deg nozzle configuration.

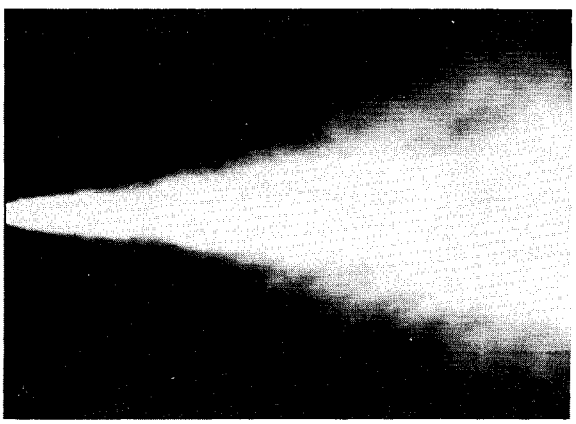

Fig. 3 Flow visualization as viewed from the XZ plane for the 45-deg nozzle configuration.

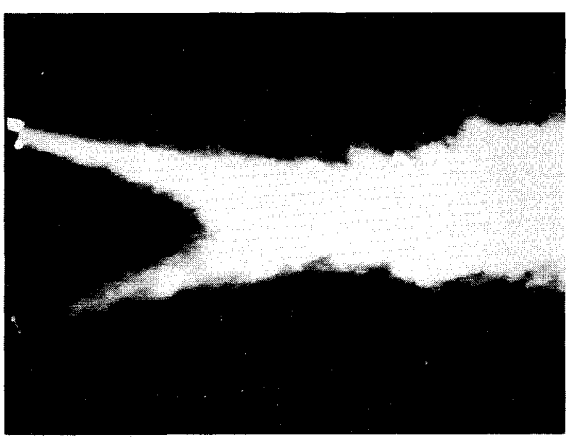

Fig. 4 Flow visualization as viewed from the XY plane for the 30-deg nozzle configuration.

To allow quantification of the jets, the smoke-laden flow was also illuminated by a single beam of coherent light. This light was supplied from a 10-mW He-Ne laser, and so light was scattered in those regions where, at any instant the jet was present, while elsewhere along the laser beam path the field remained dark (see Fig. 5). Line images were captured at a framing rate of 25 Hz using a monochrome charge-coupled device (CCD) camera. To minimize image blur the shutter speed was set to 4 ms. A total of 5000 images (i.e., 200 s) were recorded on SVHS tape for subsequent analysis using an image processing system. The line image time history at any location in the jet could then be analyzed in real-time by a microcomputer. The analysis examines either the jet boundaries (smoke present/no smoke present) or the intensity of

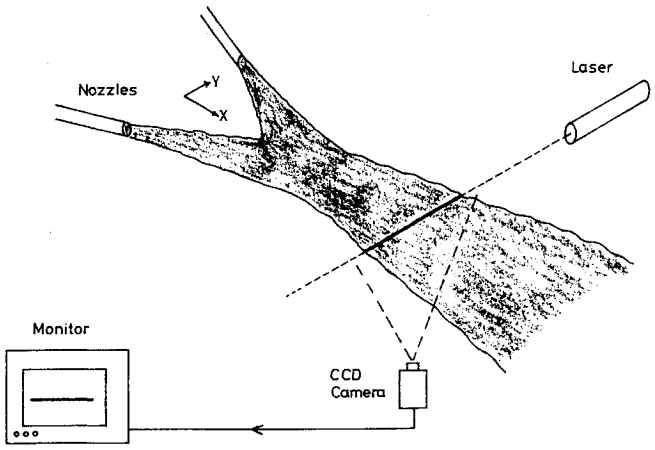

Fig. 5 Schematic representation of the layout for the laser-line analysis of the angled smoke jets.

any pixel(s) to yield intermittency and probability density functions (PDFs) of the interface. The laser and camera were both attached to a precision traversing mechanism with their positions fixed relative to each other. Spatial accuracy of this system was ±0.02 mm. Hence, the laser/camera arrangement could be traversed through the jet interaction region to buildup a complete picture of the flowfield in any cross section through the jets.

Pressure Measurements

The jet nozzle arrangement used in the flow visualization studies was also utilized for the pressure measurements as shown in Fig. 1. In these tests the two jet exit velocities were set to 14.1 m/s, giving a Reynolds number of 1.8×10^4. This value is broadly similar to the values of Rho et al.,[2] $Re = 5.2 \times 10^4$, and Rajaratnam and Khan,[4] $Re = 3 \times 10^4$. Once again, experiments were conducted for impingement angles of 30 and 45 deg, with X_0 being set to $10.33D$ in both cases. The pressures were measured using a pitot tube with the reference pressure taken to be atmospheric pressure outside the jets. The barometric pressure was also monitored so that the data could be referenced to absolute conditions if required. A pitot tube was attached to the precision two-dimensional traversing mechanism that was controlled from a computer via an Institute of Electrical and Electronics Engineers bus and stepper motor control units. The pressures were measured using a Furness transducer that had a nominal range of ±10 mmH_2O. The output voltage from this transducer was connected to an amplifier and digitized by a 10-bit A/D converter at a rate of 2 kHz and stored within the computer for postprocessing. Pitot traverses were taken across the jets in the planes of symmetry in both the Y and Z directions for downstream distances from $2D$ to $30D$. In each case the total pressure data relative to atmospheric P_t was normalized by the total pressure relative to atmospheric measured at the jet exit P_{te}. In each line of measurement across the jets, the pressure profile half-width of the jets (b_1 or b_2) was defined as the corresponding radial position where the pressure (P_t/P_{te}) had decreased to 0.5 of the maximum value.

Presentation of Results

The pressure distributions are discussed first in this article. Normalized total pressure profiles obtained in the XY plane of symmetry for the 30-deg angled jets are illustrated in Figs. 6 and 7. Likewise, the corresponding data in the XZ plane of symmetry are presented in Fig. 8. Similarly, the XY plane of symmetry pressure data for the 45-deg jets is given in Figs. 9 and 10, while Fig. 11 shows the relevant XZ plane results.

In order to examine the similarity of the total pressure profiles in the Y and Z directions at different downstream

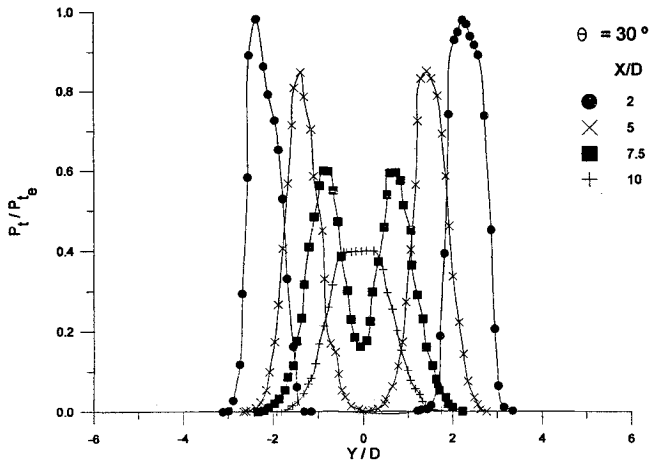

Fig. 6 Total pressure profiles normalized by the exit total pressure in the Y direction to X/D for the 30-deg angled jets.

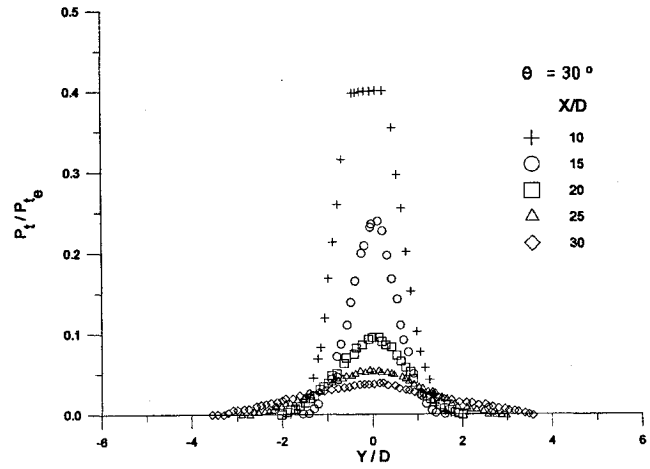

Fig. 7 Total pressure profiles normalized by the exit total pressure in the Y direction to X/D for the 30-deg angled jets.

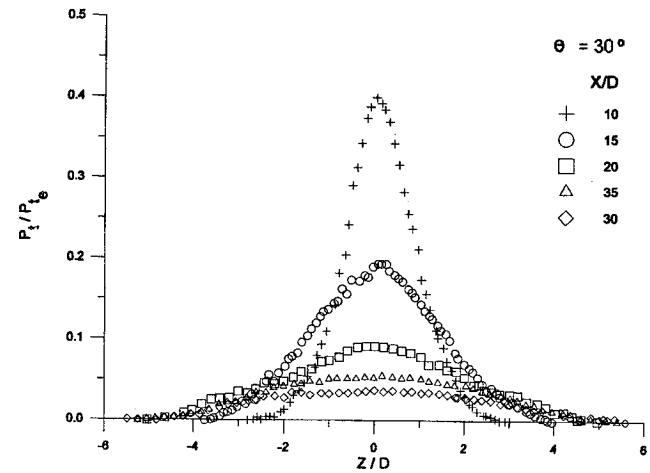

Fig. 8 Total pressure profiles normalized by the exit total pressure in the Z direction to X/D for the 30-deg angled jets.

locations, beyond the point of impingement, each P_t profile was first normalized by the maximum total pressure in that section $P_{t\max}$. Then, the spatial ordinate of the profile was normalized by the relevant half-width value, namely b_1 in the Y direction and b_2 in the Z direction. For the 30-deg jet case, Figs. 12 and 13 display these normalized values in the Y and Z directions, respectively. In a similar fashion, the 45-deg case data are plotted in Figs. 14 and 15. In addition to the

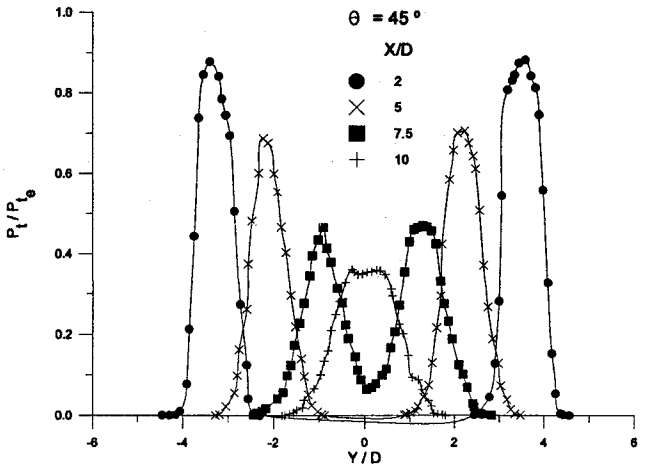

Fig. 9 Total pressure profiles normalized by the exit total pressure in the Y direction to X/D for the 45-deg angled jets.

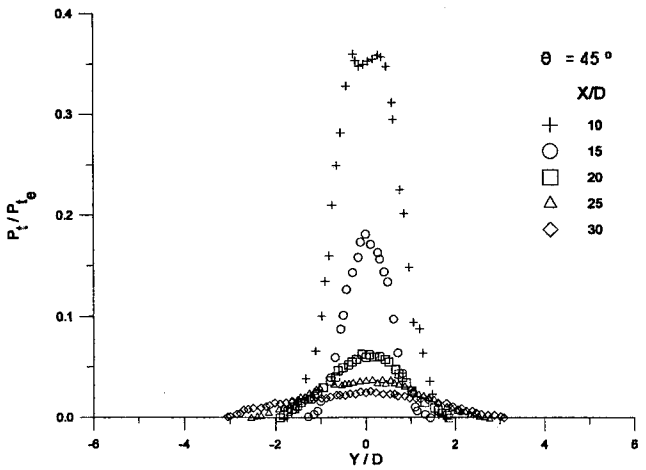

Fig. 10 Total pressure profiles normalized by the exit total pressure in the Y direction to X/D for the 45-deg angled jets.

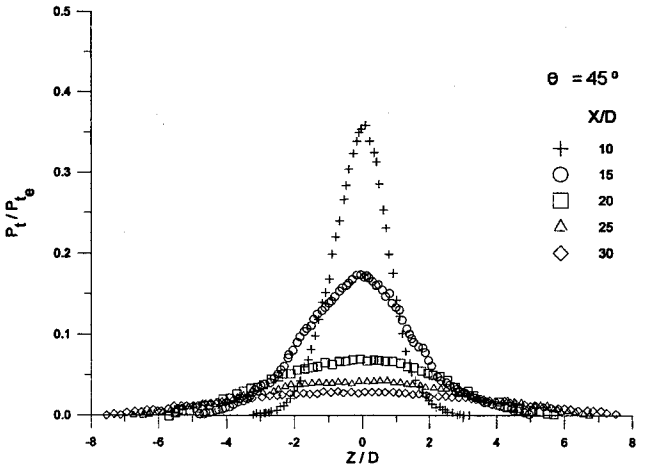

Fig. 11 Total pressure profiles normalized by the exit total pressure in the Z direction to X/D for the 45-deg angled jets.

cross-stream variations of the total pressure, the decay of the maximum P_t with downstream distance is plotted in Fig. 16 for both the 30- and 45-deg case. In this case the P_t measured on the jet centerline is normalized by P_{te}, the total pressure at the nozzle exit. The variation of the lateral b_1 and transverse b_2 half-widths, as a function of downstream distance (X/D) are plotted in Fig. 17. Finally, in Fig. 18 the average mixing cross section of the present data for the 30- and 45-deg cases is presented and compared to the data of Rho.[2]

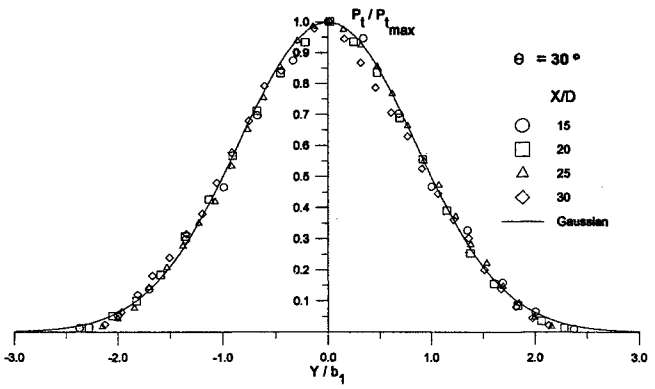

Fig. 12 Nondimensional profiles of total pressure in the Y direction across the 30-deg angled jets.

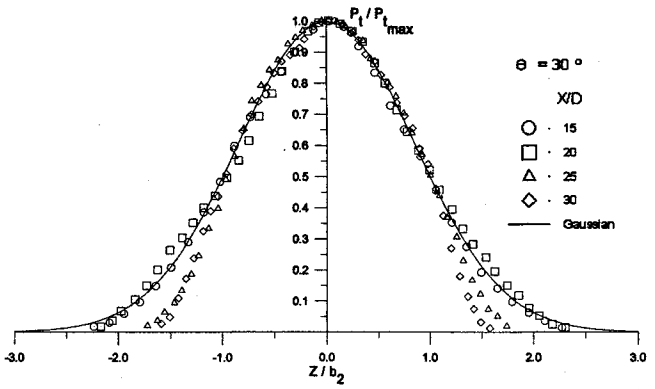

Fig. 13 Nondimensional profiles of total pressure in the Z direction across the 30-deg angled jets.

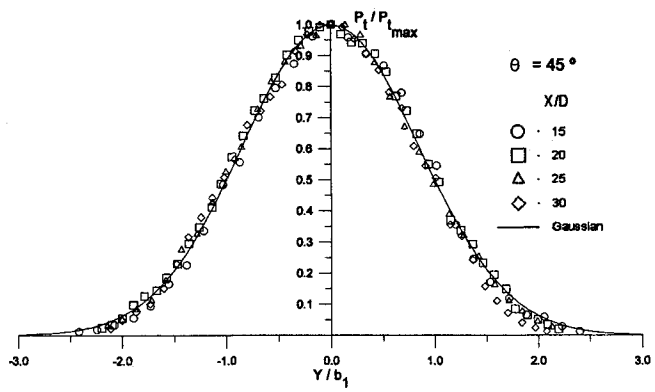

Fig. 14 Nondimensional profiles of total pressure in the Y direction across the 45-deg angled jets.

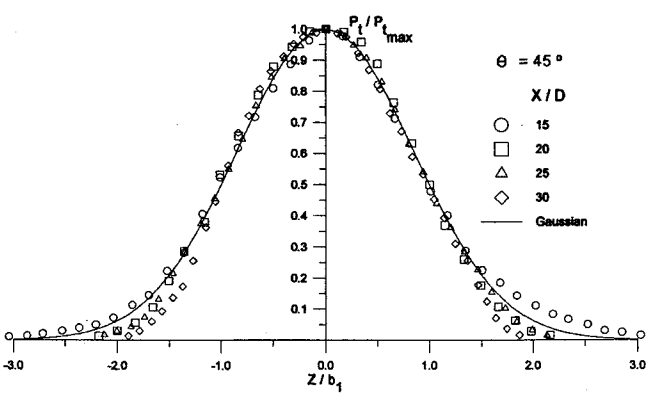

Fig. 15 Nondimensional profiles of total pressure in the Z direction across the 45-deg angled jets.

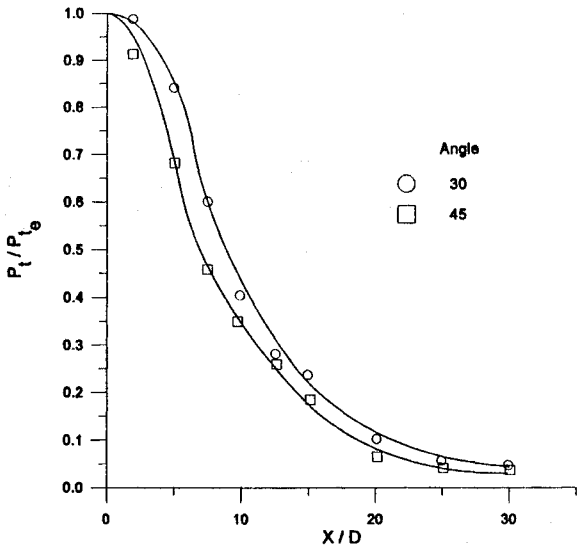

Fig. 16 Decay of centerline total pressure with downstream distance for the two jets.

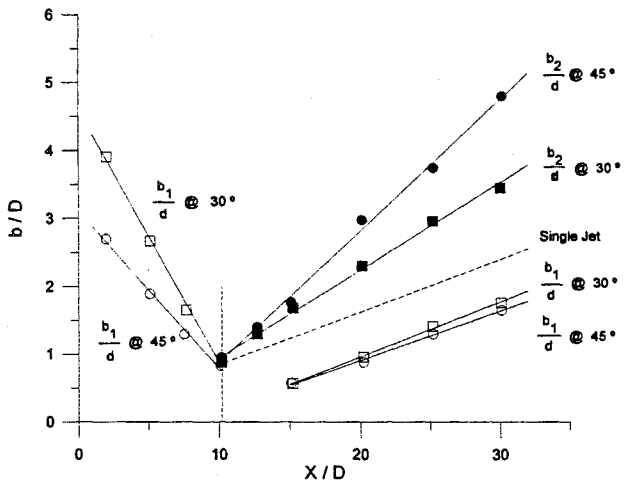

Fig. 17 Variation of half-width of the jets.

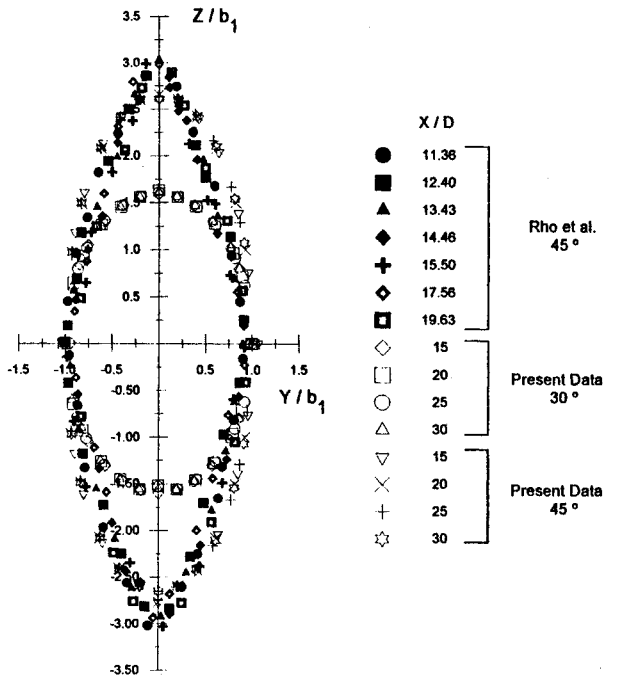

Fig. 18 Mixing cross section.

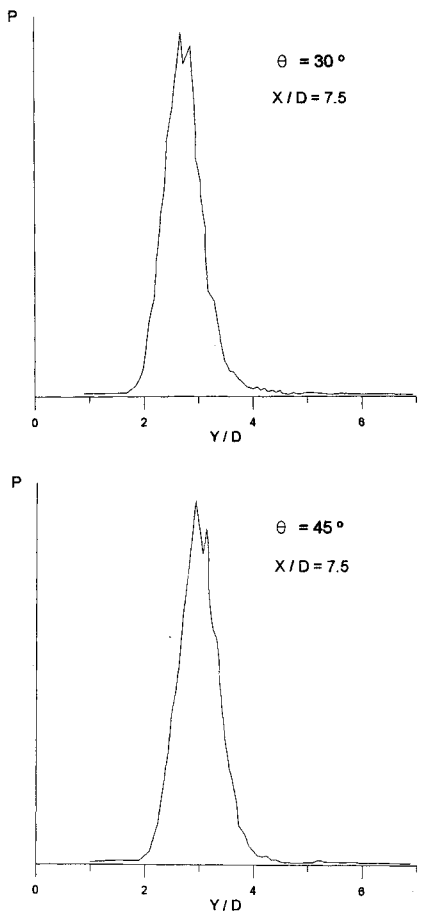

Fig. 19 Probability density distribution of the jet interface at X/D = 7.5 for the two jet cases.

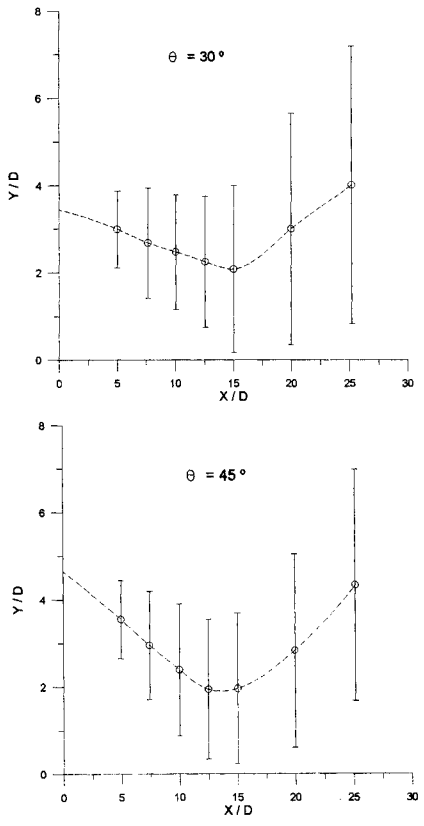

Fig. 20 Mean outside interface location and overall width of the interface for both jet cases.

Some typical quantitative smoke visualization data are presented in Figs. 19 and 20. Figure 19 shows the probability density distributions for the location of the jet/external fluid interface in the Y direction at $X/D = 7.5$ for the 30- and 45-deg cases. This was accomplished by measuring the pixel location at the jet edge, which occurred in the 5000 sequential images. From this time history the PDF of the edge position was determined. Fig. 20 illustrates the mean interface location, which coincides with the peak of the PDFs and its variation in the Y direction. This variation in location provides an estimate of the overall width (defined as the distance between the limits of the PDF profiles) of the interface for the two jet configurations.

Discussion of the Results

Considering first the pressure profile data for the 30-deg jets, it can be seen from the XY plane data in Fig. 6 that two distinct jets exist in the region from $X/D = 2$ to $X/D = 7.5$. These normalized profiles also appear to be symmetric about the respective nozzle centerline. It can be observed from Fig. 6 a narrowing of the gap between the two jet centerlines with increasing X/D. It is not until approximately $X/D = 10$ (i.e., close to the impingement location defined by the jets geometrical centerline) that the two profiles are completely merged. In this region the jets are interacting and beginning to coalesce so that, in the time mean sense, the profiles begin to resemble those of a single jet. Since the two initial jets are axisymmetric prior to impingement, the P_t profiles show an almost identical rate of spread in both the Y and Z directions. Hence, near the exit of the nozzles only the Y direction data are presented in this article. When the fluid particles reach $X/D = 15$ the normalized P_t profile in the XY plane clearly resembles that of a fully developed single jet (Fig. 7).

After impingement these jets form a fan and spread in the Z direction much more rapidly (see Figs. 2 and 3) than in the Y direction (Fig. 4), as will be illustrated later in this section. An examination of the P_t distributions in the Z direction, for the 30-deg case (Fig. 8) indicates fully developed profiles suggesting the existence of a single jet at downstream distances greater than $X/D = 10$. Note there is a discrepancy in the total pressure ratios at location $(15D, 0, 0)$. This appears to be a result of experimental error in the total pressure probe alignment in the Y and Z traverses.

Examining the normalized mean total pressure profiles acquired downstream of the jet nozzles in the XY plane from $X/D = 2$ to $X/D = 10$ for the 45-deg case (Fig. 9) a narrowing of the gap between the jet centers with increasing downstream distance is found. Also noted is the fact that the gap in the present case is larger than that in the 30-deg case. The centers are indicated by the two maxima found in the P_t traverses. It is interesting to note that a small remnant of two separate jets (two small peaks in the profile) still exists at $X/D = 10$, unlike the 30-deg case where a bluff or flat top profile was recorded. Hence, at this location lateral mixing of the jets is still very much incomplete. In Fig. 10, the P_t profiles from $X/D = 15$ to 30 clearly indicate fully merged shapes, as in the equivalent 30-deg case. The P_t profiles acquired in the vertical or Z direction for the 45-deg case (Fig. 11) also indicate an approximately symmetric profile, beyond impingement, between $X/D = 10$ and 30. Although there was a difference in the total pressure ratio for the 30-deg case, for the 45-deg case at the same location $(15D, 0, 0)$, the total pressure ratios only differed by approximately 5%.

Considering next the normalized similarity profiles for the total pressure distributions, the plots for the 30-deg jets in the Y direction (Fig. 12) beyond impingement show good similarity. The solid line shown on this and the other normalized plots represents the Gaussian profile given by

$$P_t/P_{t\max} = \exp[-0.693(Y/b_1)^2]$$

in the Y direction and

$$P_t/P_{t\max} = \exp[-0.693(Z/b_2)^2]$$

in the Z direction. The profiles in the Z direction for the 30-deg jets, in the same region (Fig. 13), show a reasonable degree of similarity in the central region near the jet axis (i.e., at distances approximately less than the corresponding half-width). However, towards the jet boundary there is considerable variation in the profile shape. This degree of nonsimilarity in the Z direction was also found by Rho et al.[2] to be present in mean longitudinal velocity profiles, as well as turbulence intensity profiles, and appeared to be associated with an increase in scatter of the higher order moments in this region (i.e., the flatness factor).

Normalized profiles in the Y and Z direction for the 45-deg jets, presented in Figs. 14 and 15, respectively, show the same trends as the 30-deg case. The Y direction profiles show good similarity with each other and fit the Gaussian profile, whereas the Z direction data shows distinctly non-Gaussian shapes, particularly beyond $X/D = 20$. Yet the amount of deviation is much less than for the 30-deg case.

The downstream decay of the normalized centerline pressures for both jet configurations (Fig. 16) clearly indicate a significant reduction in the decay rates at a downstream distance somewhere close to the geometrical impingement point. The experimental arrangement for the 45-deg angled jets was essentially the same as that used in earlier work by Rho et al. The data representing the total pressure decay for $X/D > 10$ for this case are in very good agreement with the hot-wire mean longitudinal velocity decay results presented by Rho et al.,[2] if it is assumed that the static pressure in the combined jets beyond impingement is approximately equal to that of the air outside the jets. On this basis, the velocity and total pressure decays are related by

$$U/U_e = \sqrt{(P_t/P_{te})}$$

If one now examines the development of the mean half-widths, in the downstream direction for the two cases (Fig. 17), it becomes apparent that the spread rate db/dx in the lateral Y direction, when $X/D > 10$ is very similar for the 30- and 45-deg cases (see Table 1). That is, the magnitude of the spread rate db/dx for the 45-deg case is approximately 10% smaller than b_1 for the 30-deg case. In addition, this growth rate is similar to that for a single jet issuing into still air ($db/dx = 0.0848$). This has been noted by many researchers and confirmed in the present experimental apparatus in earlier work using quantitative analysis of smoke jets.[6] On the other hand, although the half-width in the vertical Z direction is the same at the point of impingement for both jet configurations, the subsequent spread rate for the 45-deg jets was estimated to be approximately 50% greater than in the 30-deg case. In addition, the 30-deg configuration was determined to have a spread rate 52% larger than that of a single jet. This can also be observed from the flow-visualization photographs (Figs. 2 and 3). Calculating the ratio of the vertical Z spread to the lateral Y spread of the jet, one obtains 2.66 for the 45-deg case and 1.59 for the 30-deg jets.

It is also interesting to note that in the impingement region the "combined" jet shape is practically circular (i.e., $b_1 \approx b_2$ at impingement) before assuming the characteristic elliptical shape further downstream. The noncircular shape can be observed from an examination of Fig. 18, which displays the elliptical nature of these jets in the far field ($X/D \geq 15$). As the impingement angle θ increases, the length of the major axis, which represents the Z or vertical variation also increases. Although excellent agreement has been found between the present normalized pressure distributions and the velocity profiles of Rho,[2] differences in the mixing cross sec-

Table 1 Summary of spread rate data after impingement

Spread direction		Single jet	Impinging jets $\theta = 30$ deg	Impinging jets $\theta = 45$ deg	$\frac{b'_{\alpha\,30}}{b'_{\alpha\,45}}$
Y	$b'_1 = \frac{db_1}{dx}$	0.0848	0.0808	0.0726	0.899
Z	$b'_2 = \frac{db_2}{dx}$	0.0848	0.1289	0.1928	1.496
——	$\frac{b'_2}{b'_1}$	1	1.60	2.66	——

tion exist. It is believed that this deviation from ellipticity in Rho's study is a result of the nozzle geometry used in their study. Specifically, they utilized two converging nozzles that provided fluid acceleration up to the nozzle exit. The approximate impingement jet cross section found in their study was that of a rhomboid, while the present study used constant area nozzles and obtained an elliptical cross section.

Typical probability density distributions (Fig. 19) show the location of the interface between the jets and the surrounding air for the 30- and 45-deg cases at $X/D = 7.5$. This figure shows that although both profiles have a normal distribution, the coalescence of the two jets is not yet complete, as evident from the bimodal distribution in the PDFs. In addition, the mean location of the interface and the overall width of this mixing region for the two cases (Fig. 20) indicate that, beyond impingement, the jet half-width (defined by the mean location) grows at approximately the same rate as the overall width of the interface.

Summary

This article has considered the behavior of two like-impinging air jets using total pressure surveys of the mixing region, together with quantitative video analysis of smoke-seeded jets. This work has confirmed some of the findings of other workers and illustrates how the angle of the two nozzles plays a significant role in the subsequent development of the jets, particularly in the region after impingement. While the rates of decay of centerline total pressure are broadly similar for both 30- and 45-deg jets, the growth of the 45-deg jets after impingement in the plane normal to the nozzle plane is some 52% greater than in the 30-deg case. However, in the nozzle plane the growth rates are almost identical for both cases and similar to that for a single axisymmetric freejet. This growth pattern produces an elliptical mixing cross section with the extent of the major axis being over 2.5 times larger than the freejet values for the 45-deg case and approximately 60% larger for the 30-deg case. The total pressure distributions after impingement may be adequately represented by Gaussian similarity profiles in the nozzle plane, but in the plane normal to this, the data exhibit much less similarity at the edges of the jets.

Acknowledgments

The authors would like to thank Curtis W. Fox of the University of Cincinnati, Cincinnati, Ohio, for his efforts in editing of the manuscript and preparation of the graphs.

References

[1]Rho, B. J., and Kim, J. K., "Study on the Statistical Characteristics of 45-Degree Circular Cross Jet Flow," *Korean Society of Mechanical Engineering Journal*, Vol. 10, No. 1, 1986, pp. 110–120.

[2]Rho, B. J., Kim, J. K., and Dwyer, H. A., "Experimental Study of a Turbulent Cross Jet," *AIAA Journal*, Vol. 28, No. 5, 1990, pp. 784–789.

[3]Rho, B. J., Kang, S. J., Choi, J. C., and Oh, J. H., "An Experimental Analysis of the Mixing Flow Field of a Turbulent Cross Jet," *Proceedings of the Second KSME-JSME Fluids Engineering Conference*, Vol. 1, Korean Society of Mechanical Engineering, Seoul, Korea, 1990, pp. 119–124.

[4]Rajaratnam, N., and Khan, A. A., "Intersecting Circular Turbulent Jets," *Journal of Hydraulic Research*, Vol. 30, No. 3, 1992, pp. 373–387.

[5]Rajaratnam, N., and Wu, S., "Intersecting Circular Jets of Unequal Momentum Flux," *Journal of Hydraulic Research*, Vol. 30, No. 6, 1992, pp. 755–768.

[6]Toy, N., Savory, E., Shoe, B., and Disimile, P. J., "Digital Image Analysis of Two Impinging Jets," *Proceedings of the Second International Conference on Turbulence Modelling and Measurements* (Florence, Italy), 1993, pp. 425–434.